# Quench-condensed hydrogen films studied by cryogenic ToF-SIMS

Taku T. Suzuki* and Soshi Iimura

*National Institute for Materials Science,*

*1-1 Namiki, Tsukuba, Ibaraki 305-0044, Japan*

(Dated: August 2, 2024)

## Abstract

Surface melting of solidified hydrogen has attracted attention in the field of superfluidity, but the existence of surface melting of solid hydrogen itself is still controversial. In the present study, we developed cryogenic time-of-flight secondary mass spectrometry (ToF-SIMS) capable of detecting surface melting by selectively analyzing hydrogen on the outermost surface. Combined with low-energy ion scattering for well-defined film growth, we successfully investigated the surface structural transition of the quenched condensed hydrogen film grown on polycrystalline tungsten substrate below the triple point. It was found that the ToF-SIMS intensity variation of $H^+$ ions by increasing the temperature of the solid hydrogen film at a constant ramp rate (temperature-programmed ToF-SIMS) shows two prominent features: the increase accompanied by sublimation and the decrease due to the elimination of the hydrogen admolecule from the tungsten surface. Both features are well explained by the desorption of hydrogen molecules from the solid hydrogen surface. We observed no evidence of surface melting.

PACS numbers:

*Corresponding author. E-mail: suzuki.taku@nims.go.jp

## I. INTRODUCTION

Cryogenic solid hydrogen has attracted attention due to its technological importance in the storage and transportation of hydrogen as a clean energy source. It has been also an important substance as a target in various experiments, such as nuclear reactions and laser-ion acceleration.

Another interesting topic related to cryogenic solid hydrogen is the surface melting (or premelting, surface supercooling, etc) of solid hydrogen in the field of superfluidity. Since the first theoretical suggestion by Ginzburg and Sobyanin [1], a number of theoretical studies have repeatedly pointed out the possible superfluid behavior of *para* $H_2$ ($pH_2$) like helium that is the only substance showing macroscopic superfluidity [2, 3, 5–11]. These predictions essentially arise from the quantum nature of $pH_2$ with light mass and bosonic ground state ($J = 0$). From the Bose condensation temperature of an ideal Bose gas given by $3.31\hbar^2 n^{2/3}/k_B m g^{2/3}$, the appearance of the superfluidity is naively expected at a higher temperature for $pH_2$ than $^4$He, where $k_B$ is Boltzmann's constant, $m$ is the atomic mass, $n$ is the number density, and $g$ is the degeneracy of each single-particle state of a definite momentum [1, 2]. The Bose temperature of $pH_2$ is calculated to be about 6 K, which is higher than the superfluid transition temperature of $^4$He (2.2 K).

However, $pH_2$ solidifies at a triple point temperature of 13.8 K, well above the predicted superfluid transition temperature, due to the stronger intermolecular attraction than helium based on the Van der Walls force. Therefore, the suppression of the intermolecular interaction has been considered as a crucial factor for realizing superfluid $pH_2$. The second macroscopic superfluidity following helium, if realized, should provide a deeper understanding of the quantum nature of matter; therefore, the control of intermolecular interaction of hydrogen has been challenged by many researchers.

The intermolecular interaction is often weakened at a surface due to the breaking of the bond at the terminated plane. The surface melting is a consequence of this intrinsic instability of the surface, which has been observed on various surfaces [12–14]. However, the appearance of the surface melting seems to be still controversial for solid hydrogen as follows.

Several years ago, Makiuchi et al. claimed that anomalous diffusion appeared only at the top surface of a solid hydrogen thin film grown on a glass substrate, which was further suggested to be indicative of a superfluid state [15]. Before Makiuchi et al., there are also a number of studies suggesting the surface melting or similar phenomena of solid hydrogen. For example, it has been reported that the melting temperature is substantially lower than the triple point in a two-dimensional system of $p\mathrm{H}_2$ grown on a Li substrate [16]. The lower melting temperature of the surface than the bulk has also been reported for $\mathrm{H}_2$ clusters [17, 18] and a solid $\mathrm{H}_2$ film [19–22]. However, a more recent theoretical study by Boninsegni has claimed that there is no evidence that the top layer of a $p\mathrm{H}_2$ film remains liquid [23]. Furthermore, experimental studies using surface plasmon resonance have reported that the surface molten layer of solid hydrogen does not exist [24].

The striking contradiction between literature concerning the surface melting of solid hydrogen may be partly due to the absence of analysis using a technique that is sensitive both to a topmost surface and hydrogen. A few available experimental data have been obtained using hydrogen-sensitive techniques, such as neutron scattering, for powder samples to enhance the surface volume ratio [22]. However, the melting of hydrogen in those powder experiments might be affected by the confinement effect [25].

Time-of-flight secondary ion mass spectrometry (ToF-SIMS) is a well-established technique for selective analysis of surface hydrogen. Since the emitted secondary ion yield depends on the density of the target molecules on the surface of which it is composed, surface melting can be detected from the intensity change of ToF-SIMS because the density of the target molecule generally changes significantly with the phase transition. Thus, the secondary ion yield drops with surface melting as the sample temperature is gradually increased if the melting occurs (temperature-programmed ToF-SIMS). This technique has been demonstrated to be useful for detecting the surface melting on various surfaces including ionic liquids [26].

The ToF-SIMS intensity $I$ is generally dependent on the surface density of the precursor ion $C_j$ as

$$I = I_p S K_j \eta C_j, \tag{1}$$

where $I_p$ the primary ion beam current, $S$ the sputtering yield, $K_j$ the ionization rate, and $\eta$ the instrumental function. Assuming these parameters are constant except for $C_j$ before and after the structural phase transition, the ToF-SIMS intensity drops at a phase transition from solid to liquid because of the decrease of the constituent molecules density, that is $C_j$ during the phase transition. In other words, the ToF-SIMS intensity should decrease if the melting occurs, which has been confirmed for various samples including ionic liquids [26].

To the best of our knowledge, this technique has not been applied to a solid hydrogen surface. A much lower temperature is required to solidify hydrogen compared to ionic liquids, and this will be a challenge for ToF-SIMS analysis. The cryogenic technique combined with ToF-SIMS is not trivial, because ToF-SIMS requires the incidence and exit of an ion beam for measurements through apertures on the radiation shield, which remarkably reduces the cooling capability of the cryostat.

It is noted that it has been reported that the hydrogen molecules on solid hydrogen surfaces are highly mobile even at much lower temperatures than the triple point. [15, 19] This has been discussed in terms of surface diffusion of the hydrogen molecules with the activation energy being substantially smaller than the thermal activation energy of a vacancy in the bulk solid hydrogen. These mobile hydrogen molecules on the surface are not necessarily related to surface melting because the hydrogen molecules may move by hopping.

There are also reports from previous studies concerning the annealing effect of a solid $H_2$ film, which may closely related to the topic in the present study. It has been revealed that the electrical conductivity of a quench condensed-$H_2$ film increases by two orders of magnitude by the increase of the temperature from 2 K to 4.2 K. [27–29] This observation has been discussed in terms of the surface roughness. It has been discussed that the annealing effect may be caused by mobile uppermost surface layers.

In the investigation regarding the surface melting of solid hydrogen, it is important to solidify hydrogen on a clean substrate surface. This is especially the case for an ultra-thin film because the interaction of the adsorbed hydrogen with the underlying substrate surface largely affects the nature of the thin film. In fact, it has been indicated that the superfluid

properties of $p\mathrm{H_2}$ are influenced by impurities or intended dopants [3, 30]. Unfortunately, ToF-SIMS is not suitable for confirming the clean surface due to the lack of quantitation caused by the matrix effect. For this reason, we combined ToF-SIMS with low-energy ion scattering spectroscopy (LEIS) in the present study. The area of the aperture placed at the radiation shield of the cryostat for entry and exit of the ion beam was minimized by sharing the incident ion beam as well as the detector between ToF-SIMS and LEIS. This enabled successful ToF-SIMS measurements on the surface of hydrogen films solidified by quench condensation.

## II. EXPERIMENTAL AND THEORETICAL METHODS

Experiments were performed in an ultra-high vacuum (UHV) analysis chamber ($7\times10^{-9}$ Pa) configured for home-built ToF-SIMS and LEIS. ToF-SIMS and LEIS shared the ion source of electron impact type (ULVAC, FIG-5) as well as the detector that is an electrostatic hemispherical energy analyzer (VSW, CL50), as shown in Fig. 1. A schematic drawing of the entire UHV chamber and evacuation system is shown in Fig. S1 [4]. Incident ion beam was 2 keV $\mathrm{He^+}$ ion with the diameter of approximately 2 mm at the sample position in both ToF-SIMS and LEIS. The ion beam was continuous in LEIS while it was pulsed in ToF-SIMS by the pulsed electric field, with a pulse width of 500 ns and a duty ratio of 1.5%. The pulse signal for chopping and the output signal from the energy analyzer were respectively used as a start and a stop signal of a time-to-digital converter (TDC) (FAST ComTec, P7888) for obtaining ToF spectra. In ToF-SIMS, we set the pass energy and the analysis energy of the energy analyzer to 90 eV and 10 eV, respectively. Thus, the secondary ions measured in ToF-SIMS have a kinetic energy of 10 eV, which, which were accelerated to 90 eV inside the energy analyzer. The flight length corresponds to the distance between the deflector for the ion beam chopping placed in the incident beam line and the detector of the energy analyzer. In our ToF-SIMS measurement, the beam fluence was less than $10^{12}$ ion$\cdot$cm$^{-2}$ that is the typical condition for static SIMS. In both ToF-SIMS and LEIS, the incident angle of the primary ion beam and the exit angle of the secondary ions measured from the surface normal of the sample were both 45°. The hydrogen partial pressure in the UHV chamber during ToF-SIMS measurements was analyzed by quadrupole mass spectrometer (QMS, Pfeiffer Vacuum, Prisma).

We exposed a clean polycrystalline tungsten foil of thickness 0.1 mm (purity: 99.95%, Nilaco, Japan) cooled below 4 K to hydrogen gas ($H_2$, HD, or $D_2$) to prepare the quench condensed - hydrogen film. The surface of the tungsten foil was preferentially parallel to {100} due to the rolling textures. The purity of the $H_2$, HD, and $D_2$ gases was 99.99999%, 97%, and 99.995%, respectively (Suzuki Shokan Co., Ltd). Before the hydrogen film growth, the W substrate surface was cleaned by a combination of flash heating to above 1800 K in UHV and 2 keV $Ar^+$ ion sputtering. After repeated cycles of the surface cleaning procedure, we successfully confirmed the clean W surface by LEIS (Fig. S2 [31]). The hydrogen partial pressure during the exposure was controlled to be $1.33\times10^{-7}$ Pa for 0.1 L or less, $1.33\times10^{-6}$ Pa for over 0.1 L to 2 L, $1.33\times10^{-5}$ Pa for over 2 L to less than 25 L, and $1.33\times10^{-4}$ Pa for over 25 L, where 1 L = $1.33\times10^{-4}$ Pa·s. The temperature-programmed ToF-SIMS measurements were started within 5 minutes of hydrogen exposure unless otherwise specified.

Hydrogen gas for quench condensation was introduced into the analysis chamber through a variable leak valve. The $H_2$ gas was supplied either directly from a cylinder or from a homemade ortho-para converter that was constructed according to the literature. [32, 33] The ortho-para converter consisted of a copper tube (1/8 inch diameter, 1 m length) into which we put iron (III) hydroxide powder (Aldrich, catalyst grade, 30-50 mesh). It was attached to the cold head of the Gifford MacMahon (GM) closed-cycled He refrigerator (SHI, SRDK-205E). The flow rate of hydrogen gas was 50 Pa·L/s at temperatures below 40 K. After the pressure in the tube reached 1.5 atm, hydrogen in the copper tube was frozen with the refrigerator cold head cooled below 4 K, and this temperature was maintained for several hours. Finally, the hydrogen gas that evaporated from the copper tube was used for the film growth of solid hydrogen. The ortho-para conversion rate is estimated to be more than 90%. [32, 33]

We used a GM refrigerator (Iwatani, HE05) together with a homemade sample stage and a radiation shield to construct a UHV-compatible cryostat that allowed sample cooling to below 4 K during ToF-SIMS and LEIS measurements (Fig. 2). The thermal shield around the sample, the shape of which is shown by the solid black line in Fig. 2, is retractable to allow the sample exchange through the load-lock chamber. The sample was electrically

floated for flash heating of the sample by electron bombardment and also to monitor the primary ion beam current.

The sample temperature was measured by a silicon diode sensor (Lake Shore, DT-670-SD-1.4H) placed near the sample, which was calibrated by the manufacturer from 1.4 K to 500 K. The temperature deviation between the read temperature of the Si diode sensor and the actual sample surface temperature is corrected by separate measurements on superconducting transition of a polycrystalline Nb foil. The thickness of the Nb foil was 0.1 mm, which was the same as that of the W foil for the growth of the solid hydrogen film. The nominal superconducting transition temperature of Nb (9.25 K) was confirmed beforehand by a SQUID magnetometer (Quantum Design, Inc., MPMS-XL) as shown in Fig. S3 [34]. It was observed that the read temperature of the silicon diode sensor at the superconducting transition temperature of the Nb film (9.25 K) was 8.4 K (Fig. S4 [35]). In our temperature calibration, this temperature difference (0.85 K) is added to the reading temperature of the silicon diode sensor. Even after this temperature calibration, there should still be a temperature difference between the actual sample surface temperature and the calibrated temperature. The effect of this temperature difference will be discussed in the Results and Discussion section.

Density functional theory (DFT) calculations were performed with VASP code [36–38] using the PBEsol [39] exchange-correlation functional. We used cutoff energy of 550 eV and a $k$-point sampling of 9×9×1. In order to have an accurate description of the interaction between hydrogen and the tungsten surfaces, we considered Van der Waals-dispersion energy-correction by S. Grimmes (DFT-D3 method) [40, 41]. The structure model of W(100) consists of six-layer slabs, where all short-bridge and three-fold sites on the surface are fully occupied by adsorbed hydrogen atoms and one a hydrogen molecule is $\sim$1.8$\mathring{A}$ above the hydrogen atom layer [42]. All of the atoms were relaxed during the geometry optimization procedure except the bottom two layers which were held fixed to the bulk geometry. 2×2 supercell for the surface and a 30.0 $\mathring{A}$ vacuum in the $c$-direction are used. The resultant lattice constants of the model structure are $a$=$b$=6.37400 $\mathring{A}$ and $c$=38.06750 $\mathring{A}$. The desorption energy of the hydrogen molecule on the hydrogen atom layer was estimated as energy difference between the fully relaxed structure and the structure in which the hydrogen molecule

is $\sim$13 $\mathring{A}$ above the hydrogen atom layer (see the bottom of Fig. 8). The latter structure was determined by placing the hydrogen molecule 1 $\mathring{A}$ away from the stable position in the $c$ direction. The total energy was 1.5 meV lower than the sum of total energies of fully hydrogen-atom-covered W(100) slab model and isolated hydrogen molecule, suggesting that our calculations are accurate to this energy order.

## III. RESULTS AND DISCUSSION

Figure 3 shows ToF-SIMS spectra of a tungsten surface exposed to HD of 100 L. During the exposure and the following ToF-SIMS measurement, the sample temperature was kept below 4 K. It has been indicated that the emission of $H^+$ and $D^+$ ions by keV energy $He^+$ ion impact is attributed to both the kinetic sputtering and the potential sputtering [43]. The W-derived cation at a mass-to-charge ratio ($m/z$) of about 200 is composed of several components including hydrated tungsten ($W-(H_3O)^+$) and protonated tungsten ($W-H^+$) in addition to tungsten mono-cation ($W^+$).

Figure 4 shows $H^+$ intensity of ToF-SIMS in the temperature-programmed ToF-SIMS measurement. The sample was prepared by exposing it to a normal $H_2$ atmosphere below 4 K. The measurement was performed by raising the sample temperature at the constant rate of 2 K/min from the quench condensation temperature. We observed substantial enhancement of $H^+$ ion emission by the increase of the sample temperature, as shown in Fig. 4. The peak position with a small exposure of 0.3 L was about 25 K, which shifts to lower-temperature side with larger exposure. Looking more closely, one notices that the onset position of the peak (labeled (i) in Fig. 4) shifts to a lower temperature side with increasing exposure, while the decreasing slopes of the peak are shared among the different exposures resulting in the peak elimination at the identical temperature (labeled (ii) in Fig. 4). The shift of the peak onset position (i) was almost complete at 25 L, where the peak onset position reached below 5 K. Thus, the peak onset position (i) shows no shift with further exposure above 25 L, which was confirmed upto 360 L (not shown).

Desorption of hydrogen from the surface during ramping of the sample temperature occurs not only at the sample surface, but also at other parts of the cryostat, such as the second

stage of the refrigerator. It is noted that an overwhelming fraction of hydrogen molecules adsorbs on the colder parts of the cryostat. However, the hydrogen molecules adsorbed on the parts other than the sample surface are not detected by ToF-SIMS because the ionization of the hydrogen molecule required for being detected takes place only at the impingement position of the incident $He^+$ ion beam. Note that the diameter of the incident $He^+$ ion beam (about 2 mm) was much smaller than the sample size ($10\times10$ mm$^2$).

We observed essentially no difference between normal $H_2$ and para $H_2$ in the temperature-programmed ToF-SIMS measurements (Fig. S5 [44]). Thus, the intensity variation of the $H^+$ ion observed in Fig. 4 is not related to the nuclear spin isomer effect.

The temperature-programmed ToF-SIMS result of the $D_2$ film shown in Fig. 5 is quite similar to that of the $H_2$ film in Fig. 4. The measurement conditions, such as quench condensation temperature and temperature ramping rate, were the same between the measurement for $H_2$ (Fig. 4) and $D_2$ (Fig. 5). Similar to $H_2$, there are two prominent features in the temperature-programmed ToF-SIMS result: the peak onset shift with exposure amount labeled (i) and the peak elimination at the same temperature among the different exposure amounts labeled (ii).

A closer look reveals a distinct isotope effect in the temperature of the peak onset position, which is summarized in Fig. 6 for the exposure amount of 100 L. The onset temperatures of the hydrogen peak in Fig. 6 are, in order from lowest to highest, $H_2$, HD, and $D_2$, which are 4.6 K, 5.2 K, and 5.9 K, respectively, for the half-maximum value. Since the increase in ToF-SIMS intensity from these onset temperatures is attributed to the densification of the hydrogen film as discussed below, the structural transition is discussed below using the onset temperature of the hydrogen peak.

Those onset temperatures (4.6 K, 5.2 K, and 5.9 K for $H_2$, HD, and $D_2$, respectively) are correspond to the saturated vapor pressure of solid hydrogen for the pressure of $10^{-4}$ Pa estimated from the following Eqs. (2)-(4). This saturated vapor pressure value is consistent with the hydrogen partial pressure around those temperatures measured by QMS shown in Fig. 7.

The solid-vapor saturation pressure of normal $H_2$ ($Q_{H2}$) is shown to be approximately expressed by [45]

$$lnQ_{H2} = 13.94 - 97.88/T. \tag{2}$$

The expression is applied to the temperature range from 2.5 to 4.5 K in which the constant sublimation energy (813.8 J/mol) is assumed. It is noted that this value is close to the binding energy of the hydrogen solid. Similarly, the solid-vapor saturation pressure of HD ($Q_{HD}$) and normal $D_2$ ($Q_{D2}$) are approximately expressed by

$$lnQ_{HD} = 14 - 120/T \tag{3}$$

and

$$lnQ_{D2} = 15.91 - 147.2/T, \tag{4}$$

respectively [45]. The applicable temperature ranges are 3.4-4.3 K and 3.8-5.3 K for the same reason as $H_2$, respectively. The temperatures for $H_2$, HD, and $D_2$ estimated for the pressure of $10^{-4}$ Pa are 4.2 K, 5.2 K, and 5.9 K using Eqs. (2)-(4), respectively. The fact that the onset temperatures of the hydrogen peak in Fig. 6 agree well with these values indicates that the onset of the hydrogen peak is due to the sublimation, although it is slightly out of the applicable temperature range. Since the sublimation energy involved in Eqs. (2)-(4) corresponds to the binding energy of a solid, the desorption of hydrogen molecules from the surface should take place on a solid surface (sublimation), not on a liquid surface (evaporation).

Because a further elevation of the temperature enhances the sublimation of hydrogen from the surface, the falling edge of the hydrogen peak reflects the decrease of the surface hydrogen concentration due to the desorption from the surface. Thus, the falling edge temperature is considered to reflect the hydrogen molecule - surface bond strength. To verify this assumption, we estimated the desorption energy of the hydrogen molecule from a fully hydrogen-atom-covered W(100) surface by DFT calculations. Figure 9 is a result of nudge elastic band technique and plots the total energy against the location of a hydrogen molecule along the path leading from the top of surface to vacuum. There is no activation barrier, and the energy difference between the initial and final states is calculated to be 78 meV.

The desorption energy of a molecule can also be estimated from the desorption temperature of the molecule by using Readhead equation: [47]

$$-\frac{d\theta}{dT} = \frac{A}{\beta}\theta^m e^{(\frac{-E_d}{RT})}, \tag{5}$$

where $\theta$, $T$, $A$, $\beta$, $m$, $E_d$, $R$ are surface coverage, temperature, pre-exponential factor, heating rate, desorption order, desorption energy, and gas constant, respectively. By substituting $A = 10^{13}$ s$^{-1}$, $\beta$=2 K/min, $m$=1, $E_d$=0.078 eV, $R = 8.617\times10^{-5}$ eV K$^{-1}$ into the equation, the falling of the hydrogen peak is calculated to ∼30 K, which agrees well with the experimental value shown in Fig. 4. Therefore, it is evident that the falling of the hydrogen peak at ∼30 K reflects the desorption energy of hydrogen molecule from the fully hydrogen-atom-covered W(100) surface.

The vapor pressure of hydrogen is not negligible at 3-4 K in UHV, which is the lowest achievable temperature in the present study. Therefore, it is crucial to discuss the adsorption/desorption balance at the sample surface during the film growth as well as the measurement. From Eq. (2), it is estimated that the saturated vapor pressure of hydrogen ($H_2$) is $1\times10^{-5}$ Pa at 3.8 K, which is close to the exposure temperature in hydrogen film growth. The hydrogen pressure introduced into the chamber ($1\times10^{-4}$ Pa) for hydrogen film growth of over 25 L was much higher than this pressure; therefore, the hydrogen film thickness increases with the exposure time in the initial stage of film growth. As the film thickness increases, the film growth rate is likely to decrease due to the limited thermal conductivity of the hydrogen film itself, because it is exposed to room temperature through the aperture of the thermal shield. Since the vapor pressure is exponentially dependent on the temperature, which is not negligible in our setup, the thermal radiation from the room temperature part is considered to give an upper limit of the hydrogen film thickness. Indeed, we observed that the W-derived signal of ToF-SIMS still appears even after very large exposures such as 600 L (not shown). In our calculation for depth profiling of the defect creation probability using the close-encounter probability method [48], it is estimated that the 2 keV $He^+$ ion can create defects in the solid hydrogen film up to 200 nm depth. By considering the energy loss in the collisional cascade approaching the surface, the upper limit of the hydrogen film thickness is estimated to be far below 200 nm.

In the initial stage of the temperature-programmed ToF-SIMS measurement, which was started immediately after the hydrogen film growth by the exposure of 100 L, the hydrogen partial pressure remains at about $1\times10^{-4}$ Pa up to 6 K as shown in Fig. 7. This is a consequence of the balance between the evacuation rate and the desorption of hydrogen from some parts of the cryostat, whose area is much larger than the sample surface. Since the vapor pressure of hydrogen is estimated to be below $1\times10^{-4}$ Pa up to the onset temperature of the ToF-SIMS peak where sublimation is considered to start (about 4.2 K); hence the hydrogen film thickness is mostly maintained.

Since the saturated vapor pressure of hydrogen in UHV is not negligible at the lowest achievable temperature (3-4 K) in our setup, the temperature-programmed ToF-SIMS result is assumed to depend on the pressure of hydrogen in the chamber. This point was investigated by controlling the hydrogen partial pressure in the chamber. Figure 9 shows the comparison between with and without the inlet of $D_2$ gas (partial pressure: $1\times10^{-4}$ Pa) during the ToF-SIMS measurement. The actual $D_2$ pressure during the measurement around the peak temperature position (5-8 K) is estimated to be about $2\times10^{-4}$ Pa and $1\times10^{-4}$ Pa with and without the $D_2$ gas inlet, respectively, by referring to the hydrogen partial pressure data shown in Fig. 7. It is observed that the onset temperature of the ToF-SIMS peak differs each other by about 0.6 K, which is consistent with the sublimation temperature difference estimated by Eq. (4).

It is observed in Fig. 9 that the $D^+$ intensity with the $D_2$ gas inlet is significantly larger than that without the $D_2$ gas inlet below the peak temperature. This is due to the densification of the film that occurs under the hydrogen atmosphere as discussed below. Since the densification of the hydrogen film in the $D_2$ atmosphere is continuous up to the sublimation temperature, the ToF-SIMS peak is less pronounced with the $D_2$ gas inlet.

To summarize, the hydrogen intensity variation in the temperature-programmed ToF-SIMS curve shows two features: the intensity increase shifting to lower temperature with the exposure amount ((i) in Figs. 4 and 5) and the elimination of the peak at the identical position among different exposures ((ii) in Figs. 4 and 5). The former is due to the sublimation of

hydrogen and the latter is due to the desorption of hydrogen admolecules contacting to the atomic hydrogen layer grown on the tungsten surface. Since both phenomena take place on a solid surface and no indication suggesting liquid hydrogen is observed, the possibility of surface melting at the solid hydrogen surface is ruled out.

There should be a deviation between the calibrated temperature and the actual sample surface temperature at temperatures lower than the superconducting transition temperature of Nb that was used for the temperature calibration. We believe that this temperature deviation should not be so large enough to change the conclusion since the sublimation temperature estimated using this temperature calibration is consistent with that estimated from the hydrogen partial pressure measured by QMS shown in Fig. 7.

The mechanism of the increase in hydrogen intensity by sublimation in temperature-programmed ToF-SIMS is discussed below. Figure 10 shows the ToF-SIMS intensity of $H^+$ and W-derived mono-cations as a function of exposure to normal $H_2$ atmosphere below 4 K. The intensity variation of $H^+$ and W-derived mono-cation is similar in the exposure range above 1 L. The similar behavior between $H^+$ and W-derived mono-cation is attributed to the protonation of the sputtered tungsten atom that affects the intensity of the W-derived mono-cations. On the other hand, the intensity variation is quite different in the initial stage of the exposure below 1 L: the intensity of the W-derived cations decreases while that of $H^+$ increases. This opposite behavior between the W-derived cations and $H^+$ indicates that those ToF-SIMS intensities are governed by the surface coverage of hydrogen. Thus, the intensity variation of the W-derived cations is the consequence of two competing effects: the decrease accompanied by the surface hydrogen coverage and the increase with the protonation of the sputtered tungsten atoms.

It is observed in Fig.10 that the $H^+$ intensity variation is saturated with an exposure of about 5 L. This indicates that the tungsten surface is completely covered by exposure to hydrogen at this exposure level. Note that the change in the temperature-programmed ToF-SIMS profile with the exposure to $H_2$ in Fig. 4 saturates at a larger exposure level of 25 L. Thus, the amount of exposure to $H_2$ needed for saturation of the change in the ToF-SIMS intensity (Fig. 10) and that in the temperature-programmed ToF-SIMS (Fig. 4) are substantially

different. The former is determined by the surface coverage by hydrogen, that is hydrogen adsorption, while the latter is determined by the sublimation as previously discussed. Thus, the discrepancy in the exposure amount dependence between these two results implies that the sublimation of the solidified hydrogen is not simply a reverse process of adsorption. We consider that the re-adsorption of sublimated hydrogen is the mechanism of densification of the quench-condensed film that is originally in a low-density state. The densification of the precursor molecules in the film enhances the secondary ion emission intensity $I$ as shown in Eq. (1). It is reasonable to expect that the ionization rate $K_j$ also changes by this densification of the hydrogen film due to the matrix effect, but the relationship between $C_j$ and $K_j$ is not clear in the present stage; hence the effect of the ionization rate is not discussed in this paper.

The proposed mechanism of the densification of the quench-condensed hydrogen film by sublimation is displayed in Fig. 11. It is well-known that the quench-condensed molecular film has generally a sherbet-like structure containing various voids, hence it is in a low-density state (Fig. 11 (a)). This is because the surface migration of a gas molecule is limited at the cryogenic temperature for the quench condensation. Thus, the hydrogen gas molecules are sticked at the firstly arrived position at the surface, which is the mechanism of the formation of the low-density film. It is noted that re-adsorption of the sublimated molecules smooths the rough surface, hence the density of the film increases (Fig. 11 (b)). Therefore, the quench-condensed molecular film is densified at the sublimation temperature while the total number of molecules in the film decreases.

Finally, the dissociative adsorption of hydrogen molecules is discussed. The hydrogen adsorption on a tungsten surface has been investigated by numerous studies both from experiment and theory. If it is limited to the cryogenic temperature adsorption which can be directly compared to the present study, however, the number of studies is limited. In the review by Ptushinskii, it is stated that the adsorption of hydrogen is dissociative in the initial stage of the adsorption on a single crystalline tungsten surface at 5 K [46]. Dissociative adsorption of hydrogen at cryogenic temperature (5 K) has been reported also by den Boer et al for W(100) [49]. We also consider that adsorbed hydrogen contacting a tungsten surface decomposes at those cryogenic temperatures. This is because the desorption temperature

in the initial stage of the hydrogen exposure agrees well with our DFT calculation assuming dissociation of hydrogen contacting the tungsten surface. It is likely that the hydrogen adsorbs in the molecular form on this atomic hydrogen layer.

## IV. CONCLUSION

Quenched condensed hydrogen films grown on a polycrystalline tungsten substrate were studied to investigate the existence of surface melting. For this purpose, we developed cryogenic ToF-SIMS combined with LEIS, sharing the incident $He^+$ beamline as well as the energy analyzer to minimize the entrance and exit apertures placed at the radiation shield of the cryostat. We successfully demonstrated ToF-SIMS analysis of the solidified hydrogen film grown on the clean tungsten substrate surface as confirmed by LEIS. We found that the hydrogen ion intensity in temperature-programmed ToF-SIMS shows two prominent futures due to sublimation and elimination of hydrogen admolecules, both well explained by the desorption of hydrogen molecules from the solid hydrogen surface, revealing no pre-melting layer on the surface.

### Data availability

Data will be made available on request.


### Acknowledgment

This work was partly supported by JSPS KAKENHI Grant No. 19K12633 and the Innovative Science and Technology Initiative for Security, ATLA, Japan, Grant Number JPJ004596. The authors appreciate the SQUID measurement by Dr. S. Arisawa.


---


[1] V. L. Ginzburg, A. A. Sobyanin, Can liquid molecular hydrogen be superfluid?, ZhETF Pis.Red. **15**, 343 (1972).

[2] H. J. Maris, G. M. Seidal, T. E. Huber, Supercooling of liquid $H_2$ and the possible production of superfluid $H_2$, J. Low. Temp. Phys. **51**, 471 (1983).

[3] M. C. Gordillo, D. M. Ceperley, Superfluidity in $H_2$ films, Phys. Rev. Lett. **79**, 3010 (1997).

[4] See Supplemental Material at URL for schematic drawing of a UHV chamber and evacuation system used in this study.

[5] M. C. Gordillo, J. Boronat, J. Casulleras, Zero-temperature equation of state of quasi-one-dimensional $H_2$, Phys. Rev. Lett. **85**, 2348 (2000).

[6] V. S. Vorob'ev, S. P. Malyshenko, Superfluid molecular hydrogen, JETP Letters **71**, 59 (2000).

[7] Y. Kwon, K. B. Whaley, Nanoscale molecular superfluidity of hydrogen, Phys. Rev. Lett. **89**, 273401 (2002).

[8] C. Cazorla, J. Boronat, Possible superfluidity of molecular hydrogen in a two-dimensional crystal phase of sodium, Phys. Rev. A **88**, 224501 (2013).

[9] T. Zeng, P. Roy, Microscopic molecular superfluid response: theory and simulations, Rep. Prog. Phys. **77**, 046601 (2014).

[10] M. Boninsegni, Superfluid response of parahydrogen clusters in superfluid $^4$He, J. Low. Temp. Phys. **201**, 193 (2020).

[11] M. C. Gordillo, J. Boronat, Supersolidity in the second layer of para-$H_2$ adsorbed on graphite, Phys. Rev. B **105**, 094501 (2022)

[12] X. Fan, X. Chen, D. Pan, Y. Liu, P. Liu, M. Li, Localization and delocationzation of surface disordering in surface mediated melting, Phys. Rev. B **104**, 134204 (2021).

[13] K. Wang, H. Z. Wu, M. K. Ge, X. G. Hou, N. Liu, J. He, W. Xi, J. Luo, Multilayer-by-multilayer surface melting of Cu(200), Phys. Rev. B **98**, 045425 (2018).

[14] I. U. Vakarelski, D. Y. C. Chan, S. T. Thoroddsen, Drag moderation by the melting of an ice surface in contact with water, Phys. Rev. Lett. **115**, 044501 (2015).

[15] T. Makiuchi, K. Yamashita, M. Tagai, Y. Nago, K. Shirahama, Multiple diffusion-freezing mechanisms in molecular-hydrogen films, Phys. Rev. Lett. **123**, 245301 (2019).

[16] M. Boninsegni, Melting of a p-$H_2$ monolayer on a lithium substrate, Phys. Rev. **70**, 125405 (2004).

[17] K. Kuyanov-Prozument, A. F. Vilesov, Hydrogen clusters that remain fluid at low temperature, Phys. Rev. Lett. **101**, 205301 (2008).

[18] M. C. Gordillo, D. M. Ceperley, Two-dimensional $H_2$ clusters: A path-integral Monte Carlo study, Phys. Rev. B **65**, 174527 (2002).

[19] E. Bloss, A. F. G. Wyatt, Surface diffusion of solid hydrogen, J. Low. Temp. Phys. **119**, 743

(2000).

[20] P. Leiderer, U. Albrecht, Investigation of quantum systems with surface plasmons and surface state electrons, J. Low. Temp. Phys. **89**, 229 (1992).t

[21] J. Classen, K. Eschenroder, G. Weiss, Structural relaxation and surface diffusion of quench-condensed hydrogen films, Physica B **219& 220**, 678 (1996).

[22] M. Maruyama, M. Bienfait, F. C. Liu, Y. M. Liu, O. E. Vilches, F. Rieutord, Quasi-liquid molecular layer at solid hydrogen surfaces, Surf. Sci. **283**, 333 (1993).

[23] M. Boninsegni, Quasi2D $H_2$ : on the verge of turning superfluid?, J. Low. Temp. Phys. **202**, 1 (2021)

[24] U. Albrecht, R. Conradt, S. Heminghaus, P. Leiderer, Wetting phenomena in films of molecufar hydrogen isotopes, Low Temp. Phys. **22**, 117 (1996).

[25] H. K. Christenson, Confinement effects on freezing and melting, J. Phys.: Condens. Matter **13**, R95 (2001).

[26] R. Souda, Matrix effects on secondary ion emission from a room-temperature ionic liquid, 1-ethyl-3-methylimidazolium bis[trifluoromethanesulfonyl]imide, J. Chem. Phys. **130**, 244707 (2009).

[27] K. Kono, U. Albrecht, P. Leiderer, Surface-state electrons on a hydrogen film. I. Annealing of the film, J. Low. Temp. Phys. **82**, 279 (1991).

[28] K. Kono, U. Albrecht, P. Leiderer, Surface state electrons on a hydrogen Film. 2. Influence of adsorbed helium films, J. Low. Temp. Phys. **83**, 423 (1991).

[29] Y. P. Monarkha, U. Albrecht, K. Kono, P. Leiderer, Helium-film-induced retrapping transition in the two-dimensional surface above an uneven solid-hydrogen, Phys. Rev. **B47**, 13812 (1993).

[30] H. Li, X. Zhang, T. Zeng, R. J. Le Roy, P. Roy, Suppression of parahydrogen superfluidity in a doped nanoscale Bose fluid mixture, Phys. Rev. Lett. **123**, 093001 (2019).

[31] See Supplemental Material at URL for low-energy $He^+$ ion scattering spectrum on the clean tungsten polycrystal surface.

[32] T. Momose, T. Shida, Matrix-isolation spectroscopy using solid parahydrogen as the matrix: application to high-resolution spectroscopy, photochemistry, and cryochemistry, Bull. Chem. Soc. Jpn. **71**, 1 (1998).

[33] A. M. Juarez, D. Cubric, G. C. King, A compact catalytic converter for the production of para-hydrogen, Meas. Sci. Technolo. **13**, N52 (2002).

[34] See Supplemental Material at URL for SQUID magnetometry data of the Nb film.

[35] See Supplemental Material at URL for the electrical resistance of polycrystalline niobium substrate as a function of the temperature measured with cooling the sample.

[36] G. Kresse, J. Furthmüller, Efficiency of ab-initio total energy calculations for metals and semiconductors using a plane-wave basis set, Comput. Mater. Sci. **6**, 15 (1996).

[37] G. Kresse, J. Furthmüller, Efficient iterative schemes for ab initio total-energy calculations using a plane-wave basis set, Phys. Rev. B **54**, 11169 (1996).

[38] P. E. Blöchl, Projector augmented-wave method, Phys. Rev. **B 50**, 17953 (1994).

[39] J. P. Perdew et al., Restoring the density-gradient expansion for exchange in solids and surfaces, Phys. Rev. Lett. **100**, 136406 (2008).

[40] S. Grimme, J. Antony, S. Ehrlich, S. Krieg, A consistent and accurate ab initio parametrization of density functional dispersion correction (DFT-D) for the 94 elements H-Pu, J. Chem. Phys. **132**, 154104 (2010).

[41] S. Grimme, S. Ehrlich, and L. Goerigk, Effect of the damping function in dispersion corrected density functional theory, J. Comput. Chem. **32**, 1456 (2011).

[42] Z. A. Piazza et al. Acta Materialia, Saturation of tungsten surfaces with hydrogen: A density functional theory study complemented by low energy ion scattering and direct recoil spectroscopy data, **145**, 388 (2018).

[43] J. Schou, B. Stenum, R. Pedrys, Sputtering of solid deuterium by He-ions, Nucl. Instrum. Meth. Phys. Res. B **182**, 116 (2001).

[44] See Supplemental Material at URL for temperature-programmed ToF-SIMS spectra on the normal-$H_2$ film and the para-$H_2$ film grown by exposing the tungsten substrate to normal-$H_2$ and para-$H_2$ atmosphere of 100 L, respectively.

[45] P. C. Souers, Hdrogen Properties for Fusion Energy (University of California Press, London England, 1986) p. 49.

[46] Y. G. Ptushinskii, Low-temperature adsorption of gases on metal surfaces (Review), Low Temp. Phys. **30**, 1 (2004).

[47] P. A. Redhead, Thermal desorption of gases, Vacuum **12**, 203 (1962)

[48] T. Fuse, O. Ishiyama, M. Shinohara, Y. Kido, Monte Carlo simulation of angular-scan spectra for coaxial impact collision ion scattering spectroscopy (CAICISS), Surf. Sci. **372**, 350 (1997).

[49] D. den Boer, O. I. Shklyarevskii, J. A. A. W. Elemans, S. Speller, Low-temperature dissociative

adsorption of H on W, Mo, and Ta surfaces studied with mechanically controllable break-junctions, Phys. Rev. B **77**, 165423 (2008).

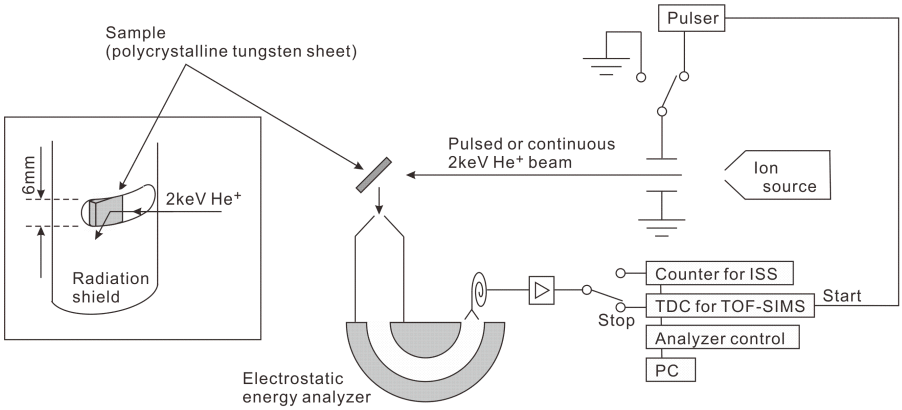


FIG. 1: Schematic of ToF-SIMS combined with LEIS. The incident ion beam line (2 keV $He^+$) and the detector (electrostatic energy analyzer) are shared between ToF-SIMS and LEIS to minimize the size of the aperture placed at the radiation shield for entry and exit of ions.

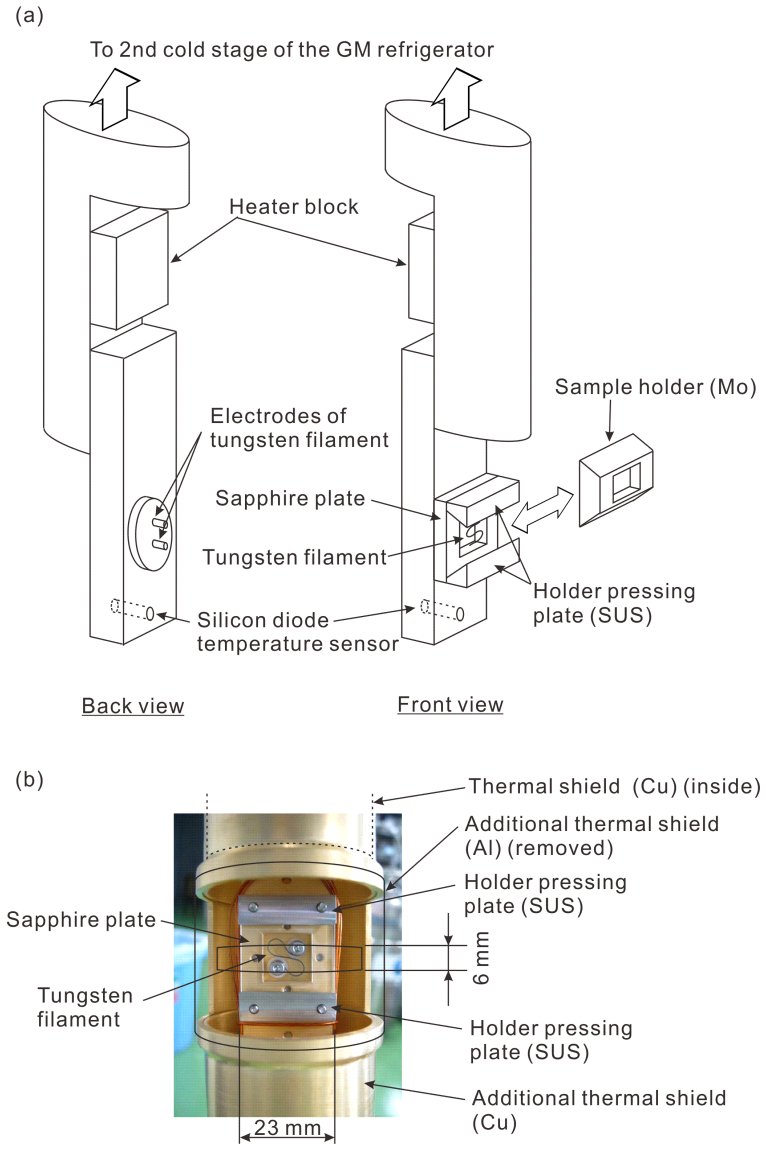


FIG. 2: (Color online) (a) Schematic of cryostat used for cryogenic ToF-SIMS. The heat-transfer rod connecting the cold head of the GM refrigerator and the sample is displayed. The sapphire plate 5 mm thick is used for electrically insulating the sample, which is heated above 1800 K by electron bombardment for surface cleaning. In temperature-programmed ToF-SIMS measurement, the heater placed in the heater block was used to raise the sample temperature at a constant rate. (b) Details around the sample station. The thermal shield made of aluminum around the sample is removed in this picture to see the sample station.

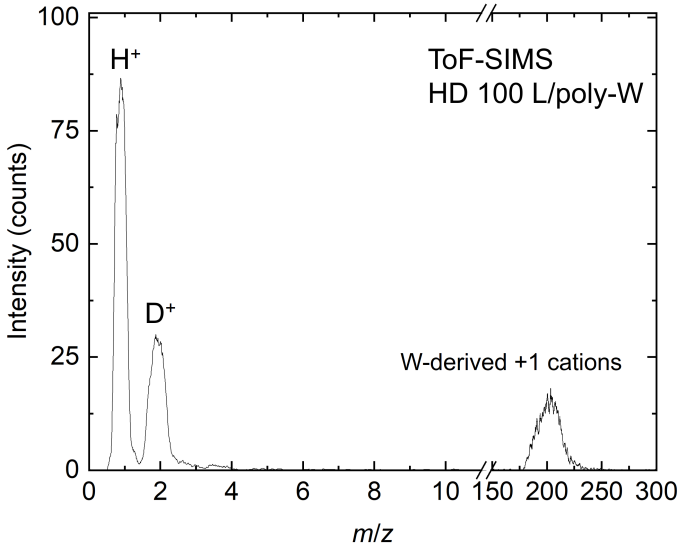


FIG. 3: ToF-SIMS spectra of quench condensed HD film grown on a tungsten polycrystal substrate prepared by exposing to the HD atmosphere of 100 L below 4 K.

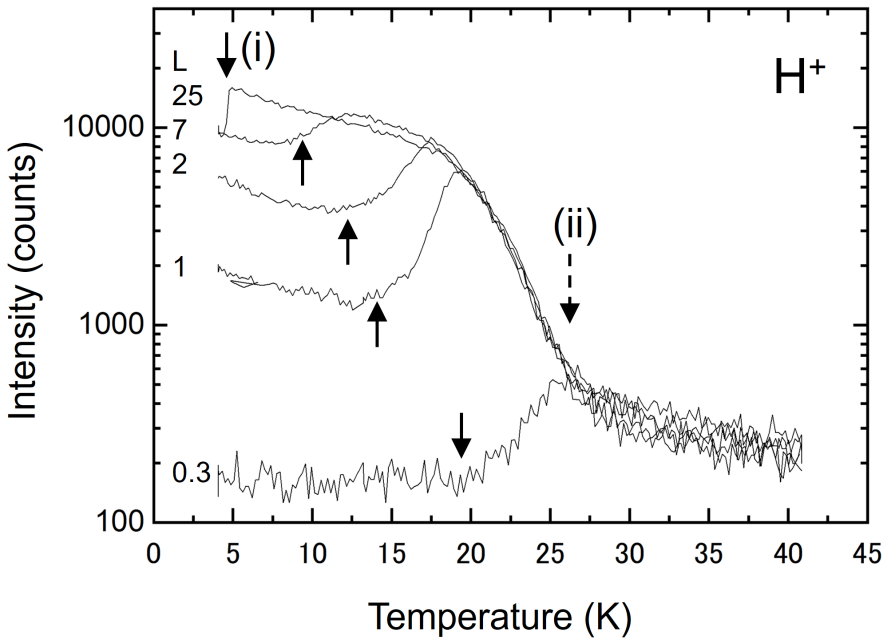


FIG. 4: Temperature-programmed ToF-SIMS spectra of $H^+$ measured on the quench condensed hydrogen film on the tungsten substrate. The peak onset temperature and the temperature at which the peak disappears are indicated by solid and dashed arrows labeled (i) and (ii), respectively.

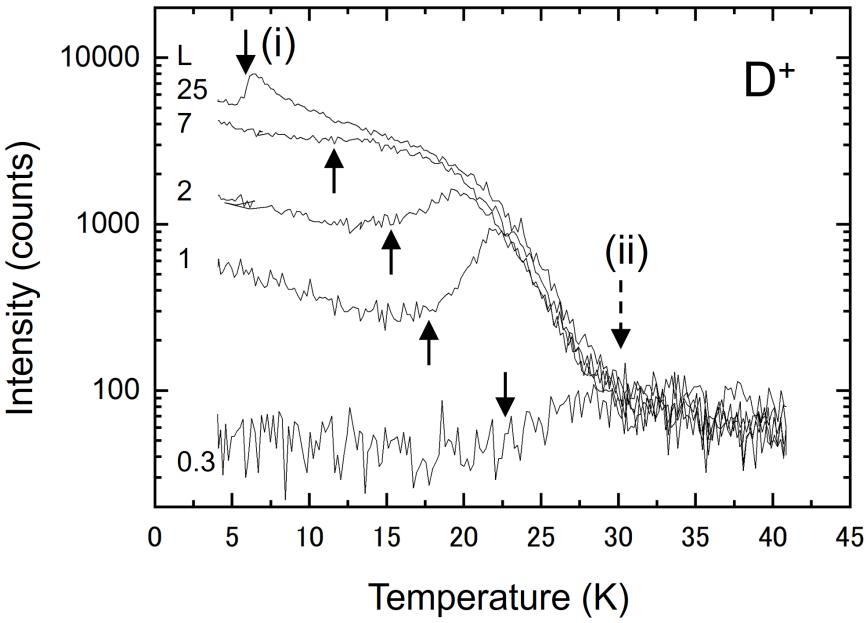


FIG. 5: Temperature-programmed ToF-SIMS spectra of $D^+$ measured on the quench condensed hydrogen film grown on the tungsten substrate. The peak onset temperature and the temperature at which the peak disappears are indicated by solid and dashed arrows labeled (i) and (ii), respectively.

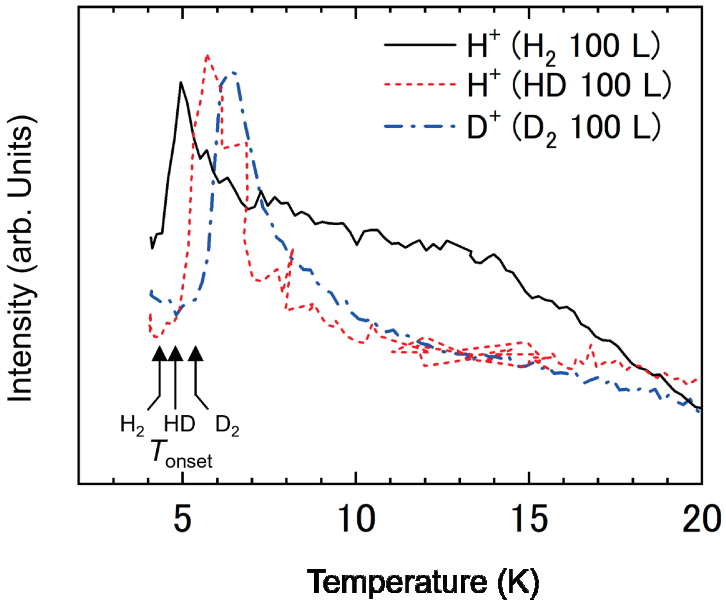


FIG. 6: (Color online) Temperature-programmed ToF-SIMS spectra of $H^+$ of the $H_2$ film (solid black curve), $H^+$ of the HD film (dotted red curve), and $D^+$ of the $D_2$ film (blue chain curve). The exposure amount is 100 L for all three measurements.

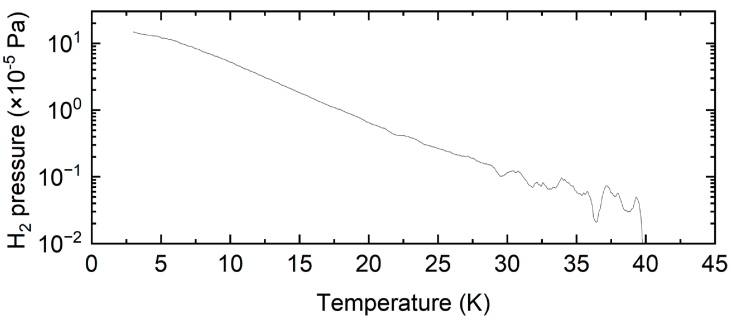


FIG. 7: The hydrogen partial pressure measured by QMS during the temperature-programmed ToF-SIMS measurement for the $H_2$ 100 L/W sample. The ToF-SIMS measurement was started immediately after the hydrogen film growth was completed.

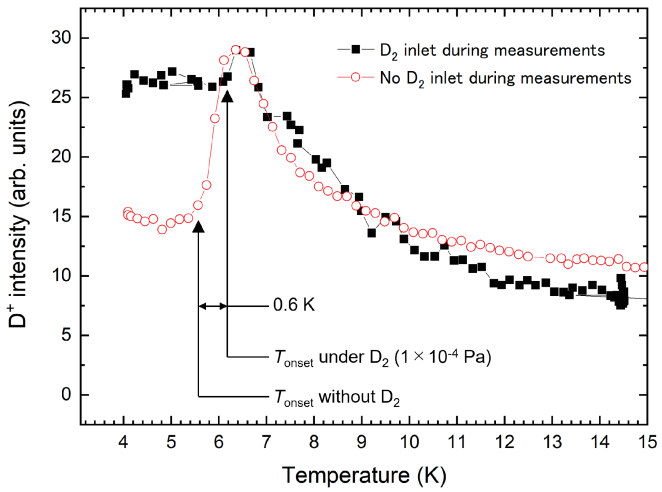


FIG. 8: (Color online) Temperature-programmed ToF-SIMS spectra of $D^+$ of the $D_2$ 100L/W sample with (solid black squares) and without (open red circles) introducing the $D_2$ gas of $1\times10^{-4}$ Pa during the measurement.

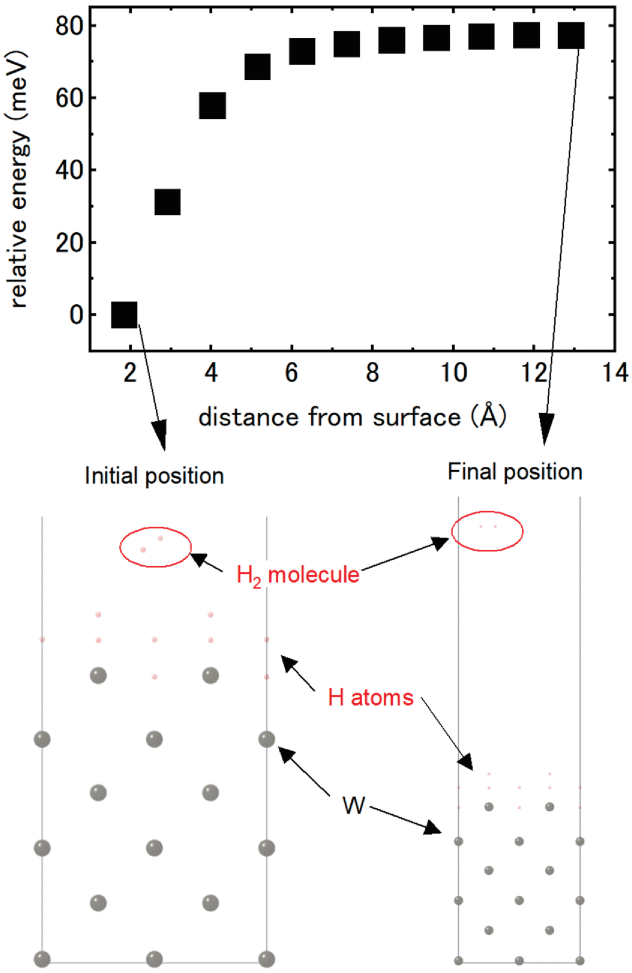


FIG. 9: (Color online) Total energy change as a function of hydrogen molecule position along the path leading from the top of the hydrogen-atom-adsorbed W(100) surface to vacuum. In the bottom of the figure, the atomic positions of initial and final states are shown. Grey and pink circles denote W and hydrogen, respectively.

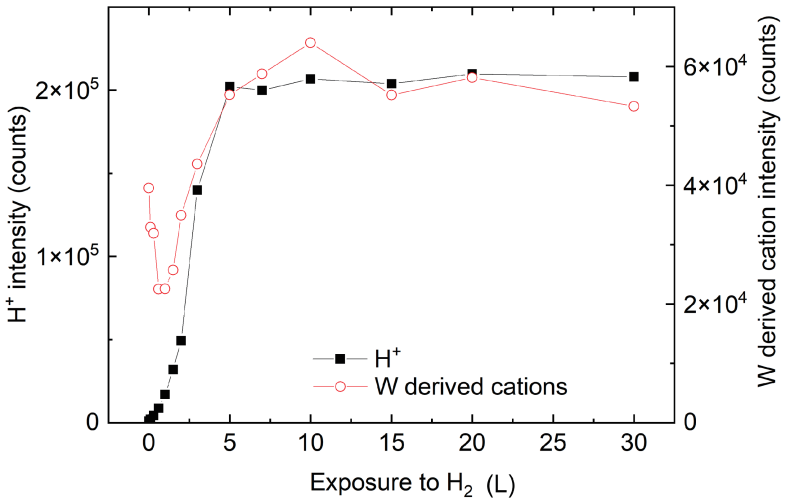


FIG. 10: (Color online) ToF-SIMS intensities of $H^+$ (solid black squares) and W-derived cations (open red circles) as a function of exposure to $H_2$ below 4 K.

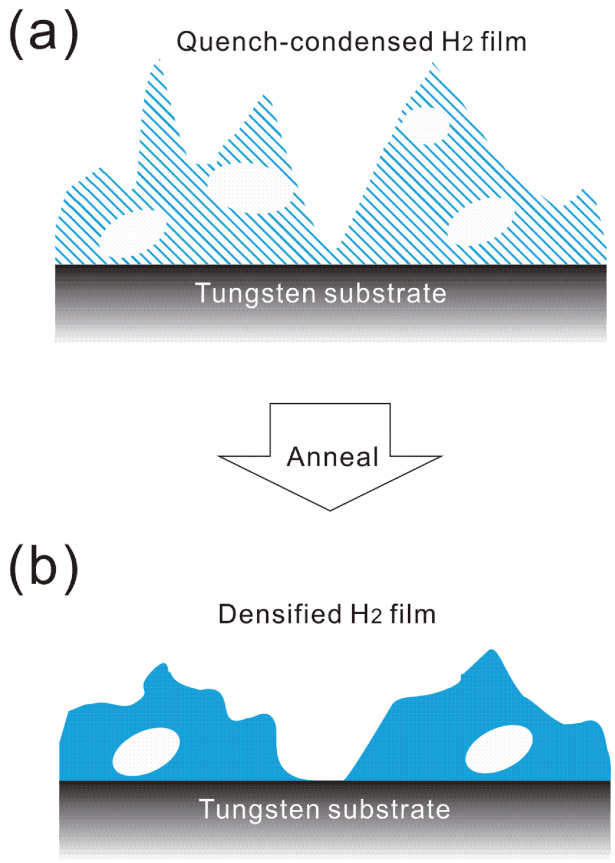


FIG. 11: (Color online) Proposed densification mechanism of a quench-condensed hydrogen film by annealing. The low-density hydrogen film grown by quench condensation (a) is densified by desorption during sublimation followed by re-adsorption after annealing (b).